TAbMEP Assessment: ICARTT H_2O Measurements

1. Introduction

Here we provide the assessment for the water (H_2O) measurements taken from three aircraft platforms during the summer 2004 ICARTT field campaign [*Fehsenfeld et al.*, 2006, *Singh et al*., 2006]. The inter-platform assessment is based upon four wing-tip-to-wing-tip intercomparison flights conducted during the field campaign. The two instruments on the DC-8 are compared using all available data from the mission. There is no H_2O data reported by the DLR Falcon due to an instrument breakdown. Recommendations provided here offer TAbMEP assessed biases for each of the measurements which can be used to unify the ICARTT H_2O data to achieve better consistency for integrated analysis. These recommendations are directly derived from the instrument performance demonstrated during the ICARTT measurement comparison exercises and are not to be extrapolated beyond this campaign.

2. ICARTT H_2O Measurements

Four different H_2O instruments were deployed on the three aircraft. Table 1 summarizes these techniques and gives references for more information.

Table 1. H_2O measurements deployed on aircraft during ICARTT

Aircraft	Instrument	Reference
NASA DC-8	Diode Laser Hygrometer (DLH)	*Diskin et al.* [2002]
NASA DC-8	Cryo-hygrometer (Cryo)	*Buck and Clark* [1991]
NOAA WP-3D	Cryo-hygrometer (Cryo)	Not available
FAAM BAe-146	Hygrometer (Hygro)	Not available

3. Summary of Results

Table 2 summarizes the assessed biases. More detailed descriptions are provided to illustrate the process for assessment of bias and precision in Sections 4.1 and 4.2 respectively. The assessed 2σ precisions normally reported in Table 2 for other species are equal to twice the highest adjusted precision value for that instrument listed in Table 5. It was not possible to derive adjusted precisions (see Section 4.2 for details) therefore no assessed 2σ precisions are reported

Table 2. Recommended ICARTT H_2O measurement treatment

Aircraft/ Instrument	Reported 2σ Uncertainty	Assessed 2σ Precision	Assessed Bias (g/kg)	Recommended 2σ Uncertainty
NASA DC-8 DLH	5%	n/a	K0=0.00732, K1=0.0259, K2=-0.0106, K3=0.000345[a]	n/a
NASA DC-8 Cryo	5%	n/a	K0=-0.00825, K1=-0.0716, K2=0.0294, K3=-0.00271, K4=0.0000777[b]	n/a
NOAA WP-3D Cryo	None	n/a	$-0.02645 - 0.01145\ H_2O_{WP3D} + 0.01134\ H_2O_{WP3D}^2$	n/a
FAAM BAe-146 Hygro	None	n/a	$0.150 - 0.0374\ H_2O_{BAe146} + 0.00163\ H_2O_{BAe146}^2$	n/a

[a] Correction in the form $K0 + K1*DLH + K2*DLH^2 + K3*DLH^3$

[b] Correction in the form $K0 + K1*Cryo + K2*Cryo^2 + K3*Cryo^3 + K4*Cryo^4$

in Table 2. Table 2 reports an assessed bias (see Section 4.1 for details) that can be applied to maximize the consistency between the data sets. The assessed bias should be subtracted from the reported data to 'unify' the data sets. For the inter-platform comparisons the assessed bias is derived from intercomparison periods only and may be extrapolated to the entire mission if one assumes instrument performance remained constant throughout the mission. No recommended 2σ uncertainty is reported since there is no assessed 2σ precision.

Figure 1 provides a quick glance of the magnitude of the bias for four H_2O instruments. The curves reflect the range of measurements for each instrument during the intercomparison period. This figure shows that the absolute bias is higher at high concentrations, however, when compared to concentration levels, the relative bias is highest at the lowest values (e.g. about 80% at 0.01 g kg^{-1} vs. about 5% at 20 g kg^{-1}). The bias correction is our best estimate of the central tendency but may not accurately reflect the bias on a point to point basis (see later discussion in Section 4.1).

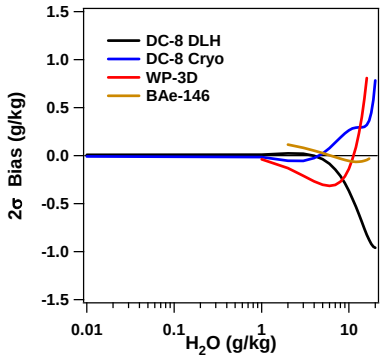

Figure 1. 2σ bias for DC-8 DLH (black), DC-8 cryo (blue), WP-3D (red), and BAe-146 (gold), as a function of H_2O level. Values were calculated based upon data shown in Table 2. The range of the curves with respect to H_2O level reflects the range of measurements of each instrument during the intercomparison period.

4. Results and Discussion

4.1 Bias Analysis

Section 3.3 in the introduction describes the process used to determine the best estimated bias. Figures 2-6 show the correlation and time series plots for each intercomparison included in this assessment. For H_2O measurements, the DC-8 DLH versus DC-8 Cryo intercomparison is taken as the standard for all H_2O analysis since both instruments are well maintained and calibrated, and the comparison was encompassed the largest range of water mixing ratio values. The standard method for determining bias as described in the introduction is not applicable for H_2O. Because the performance of the two instruments involved have very different dependence on ambient conditions, the Reference Standard for Comparison (RSC) is not taken as an average of the two. Rather it emphasizes the better performing instrument while de-emphasizes the other for a given range of conditions. The ICARTT field campaign was the first time DLH reported data for very high concentrations (> 10 g/kg) , and was thought to have some accuracy issues in that range. Therefore, the cryo-hygrometer is weighted more heavily at high concentrations. The cryo-hygrometer technique is subject to difficulties at low dew point (e.g., water/ice ambiguity, see discussion in section 4.1), thus DLH is weighted more heavily in this case. The two

instruments are weighted equally in the intermediate range, where both are known to perform well. The two instruments are weighted equally in the intermediate range, where both are known to perform well. The resulting RSC is defined as follows:

$$RSC_{H2O} = \begin{cases} \dfrac{DLH + 2\,Cryo_{DC8}}{3} & Cryo_{DC8} > 10\ g/kg \\ \dfrac{2\,DLH + Cryo_{DC8}}{3} & \text{Dew point} < -15^{\circ}C \\ \dfrac{DLH + Cryo_{DC8}}{2} & \text{All other points} \end{cases}$$

Unlike the other species, the RSC for H_2O can be considered as the better measure of the average H_2O concentration sampled by NASA DC-8 aircraft, not necessarily on a point-to-point basis. This reflects that the RSC is derived by combining measurements of differing temporal response characteristics. Using the RSC, the best representation of the bias can be determined through regression analysis as shown in Figures 8-11. This is believed to be an effective way to determine the mean bias between the measurements.

To quantify the bias for each of the four ICARTT H_2O measurements, the difference between the individual measurements and the RSC is plotted against the measurement mixing ratio in Figures 8-11. For the all instruments, polynomials are used as they can better represent the best estimate biases (black lines), over the largest concentration range. The equations for these lines are the bias and are reported in Table 3 as the best estimate bias. It is noted here that Figures 8 – 11 show large variability for all four instruments. For example, the BAe-146 bias scatter is so large that one cannot help wondering the meaning of the bias correction, other than it may better reflect the central tendency. In the case of WP-3D in Figure 10, the fit could be quite different if the data from 07/22/2004 (red) is not included. However, there is no reason for excluding it. The panel strongly recommends that the bias estimates be treated as the correction for central tendency, but may not effectively remove the potential bias on a point to point basis.

Table 3. ICARTT H_2O bias estimates

Aircraft/ Instrument	Linear Relationships	Best Estimate Bias (g/kg)
NASA DC-8 DLH	n/a	K0=0.00732, K1=0.0259, K2=-0.0106, K3=0.000345[a]
NASA DC-8 Cryo	n/a	K0=-0.00825, K1=-0.0716, K2=0.0294, K3=-0.00271, K4=0.0000777[b]
NOAA WP-3D Cryo	n/a	$-0.02645 - 0.01145\ H_2O_{WP3D} + 0.01134\ H_2O_{WP3D}^2$
FAAM BAe-146 Hygro	n/a	$0.150 - 0.0374\ H_2O_{BAe} + 0.00163\ H_2O_{BAe}^2$

[a] $K0+K1*DLH+K2*DLH^2+K3*DLH^3$

[b] $K0+K1*Cryo+K2*Cryo^2+K3*Cryo^3+K4*Cryo^4$

To better illustrate the bias variability and the complexity of the comparison, Figure 12 (a - d) shows four cases of ICARTT comparisons between DC-8 DLH and cryo ranging from boundary layer to upper free troposphere. Figure 12 (a - d) depicts DLH (red) and cryo (blue) mixing

ratios (g/kg) during level flight leg segments in the lower panel and the residual (DLH – cryo, green) in the upper panel, both as functions of time. In general, at low H_2O concentrations, the residual is fairly stable, though slightly positive (upper panel, Figure 12d), ranging between 0.04 and 0.08 g/kg. At higher H_2O the residual is larger and varies considerably more (upper panel, Figure 12a), ranging between -1.6 and -0.8 g/kg. This systematic shift in the H_2O data is captured by the best estimate bias shown in Table 3.

In addition to this systematic shift, there are other systematic differences at times not easily characterized by the estimated bias which limit the effectiveness of the bias correction based on all data. Complications can occur when there are abrupt changes in H_2O levels. This is illustrated in Figure 12b with H_2O levels that are highly variable. The residual (upper panel) has a fairly stable baseline near zero, but there are frequent and significant deviations from the baseline. One explanation for the deviations is a cryo time response lag relative to DLH. Several examples can be seen at ~19:30, 19:38, and between 19:35 and 19:36. In addition, at these times (as well as at 19:23) cryo overshoots the DLH data, resulting in the previously mentioned spikes in the residual as well as the spike at 19:23. Finally, at about 19:32 DLH and cryo are nearly anti-correlated. The time lag response issue is also present, though less dramatically, in Figure 12d between 19:31 and 19:32. Another complicating factor to the bias correction is cryo having a slower response to changes in H_2O relative to DLH. Though difficult to discern in these plots, it is noticeable when regions are expanded horizontally (e.g. Figure 12b between 19:39:30 and 19:40:00 and between 19:41:00 and 19:41:30). This detail is present when more subtle changes in H_2O occur as well. In Figure 12a the spikes in the residual at ~14:49, 14:52, 14:53, and between 14:59 and 15:00 are the result of additional structure in the DLH data that is not present in the cryo data. Finally, even when the residual is relatively constant (Figure 12c) and near zero for much of the level flight leg, there are still unexplained deviations, e.g., -0.5 g/kg at about 17:14:00. These complicating factors combine to limit our ability to effectively remove bias from the data on a point by point basis.

Another way to characterize the effectiveness of the bias correction is to test if the bias corrected relative residual, as shown in Figure 13, falls within PI reported uncertainties. In this case, both DC-8 DLH and DC-8 cryo data were corrected using the best estimate bias listed in Table 3. The overall average is <0.1% and standard deviation is 12.8%. As shown in Figure 13, however, the difference between the bias-corrected DC-8 DLH and cryo data remains to be a finite positive or negative value at various RSC values and appears to be a function of the RSC. This trend can be characterized by dividing mixing ratio levels into three regimes, i.e., less than 0.2 g/kg, between 0.2 and 1 g/kg, and above 1 g/kg, yielding different values for the standard deviation (see Table 4). Since there is substantial variability in the standard deviation after bias correction, it is likely that the bias cannot be systematically removed and no value for observed variability can be given in Table 5.

Table 4. DC-8 DLH vs. Cryo

RSC	< 0.2	0.2 ≤ RSC < 1	≥ 1
Observed Variability	-4.0 ± 16.8%	10.8 ± 10.5%	-2.8 ± 8.15%

This uncertainty is also affected by ambiguity between supercooled water and ice in the cryo measurements. This ambiguity exists for dew points between 0°C and -40°C when the cryo instrument cannot distinguish between liquid water and ice on its detection mirror. To illustrate

this ambiguity, Figure 14 shows DC-8 DLH and DC-8 cryo percent residual as a function of dew point and RSC mixing ratio (g/kg). For dew points between 0°C and -40°C the spread in the data changes (greater spread at colder dew points) as a result of the ambiguity. The upper bound of the uncertainty, shown as a black line, ranges from 0 to 40% depending on dew point. Without a systematic way to incorporate this into the bias equation, it contributes to the larger than expected uncertainty.

4.2 Precision Analysis

A detailed description of the precision assessment is given in Section 3.1 of the introduction. The IEIP precision and expected variability are summarized in Table 5. Observed variability and adjusted precision are also normally presented in Table 5, however in this case the bias between the measurements cannot be effectively removed by our procedures and the magnitude of the remaining bias may be comparable to the precision. Therefore, the observed variability analysis is unlikely to provide a reasonable assessment of the long-term precision as it was intended to. Without an observed variability, adjusted precision cannot be calculated.

IEIP procedures were applied to both the DC-8 DLH and cryo data from the entire INTEX-NA period. The DC-8 cryo data presented challenges in deriving a precision estimate due to the slow response time of the instrument. In order to derive an estimate, longer time intervals were needed (possible for entire INTEX-NA time period, but not for individual intercomparison periods). Because the DLH had a better precision than cryo and the cryo data was not ideal for this analysis, DLH was chosen as the basis for comparison with other instruments and only DLH IEIP precisions are listed for the individual intercomparison periods in Table 5.

Table 5. ICARTT H_2O precision (1σ) comparisons

Flight	Platform	IEIP Precision	Expected Variability	Observed Variability	Adjusted Precision
07/22	DC-8 DLH	1.5%	2.3%		
	WP-3D	1.8%			
07/31	DC-8 DLH	1.5%	2.1%		
	WP-3D	1.5%			
08/07	DC-8 DLH	2.4%	3.1%		
	WP-3D	2.0%			
07/28	DC-8 DLH	2.5%	7.4%		
	BAe-146	7.0%			
All flights	DC-8 DLH	1.0%	2.1%		
	DC-8 Cryo	1.8%			

4.3 Conversion Equations

The following equations were used to convert dew/frost point (T_d in K) to mixing ratio (g/kg).

$$e_w = 10^{[23.5518-(2937.4/T_d)]} \times T_d^{(-4.9283)} \qquad (4.3.1)$$

$$e_i = 10^{[11.4816-(2705.21/T_d)]} \times T_d^{(-0.32286)} \quad (4.3.2)$$

e_w = partial pressure of water vapor over water (mb)

e_i = partial pressure of water vapor over ice (mb)

$$q\ (g/kg) = \frac{622 \times e_{w,i}}{P_s - (0.378 \times e_{w,i})} \quad (4.3.3)$$

q = mixing ratio (g/kg)
P_S = static pressure (mb)

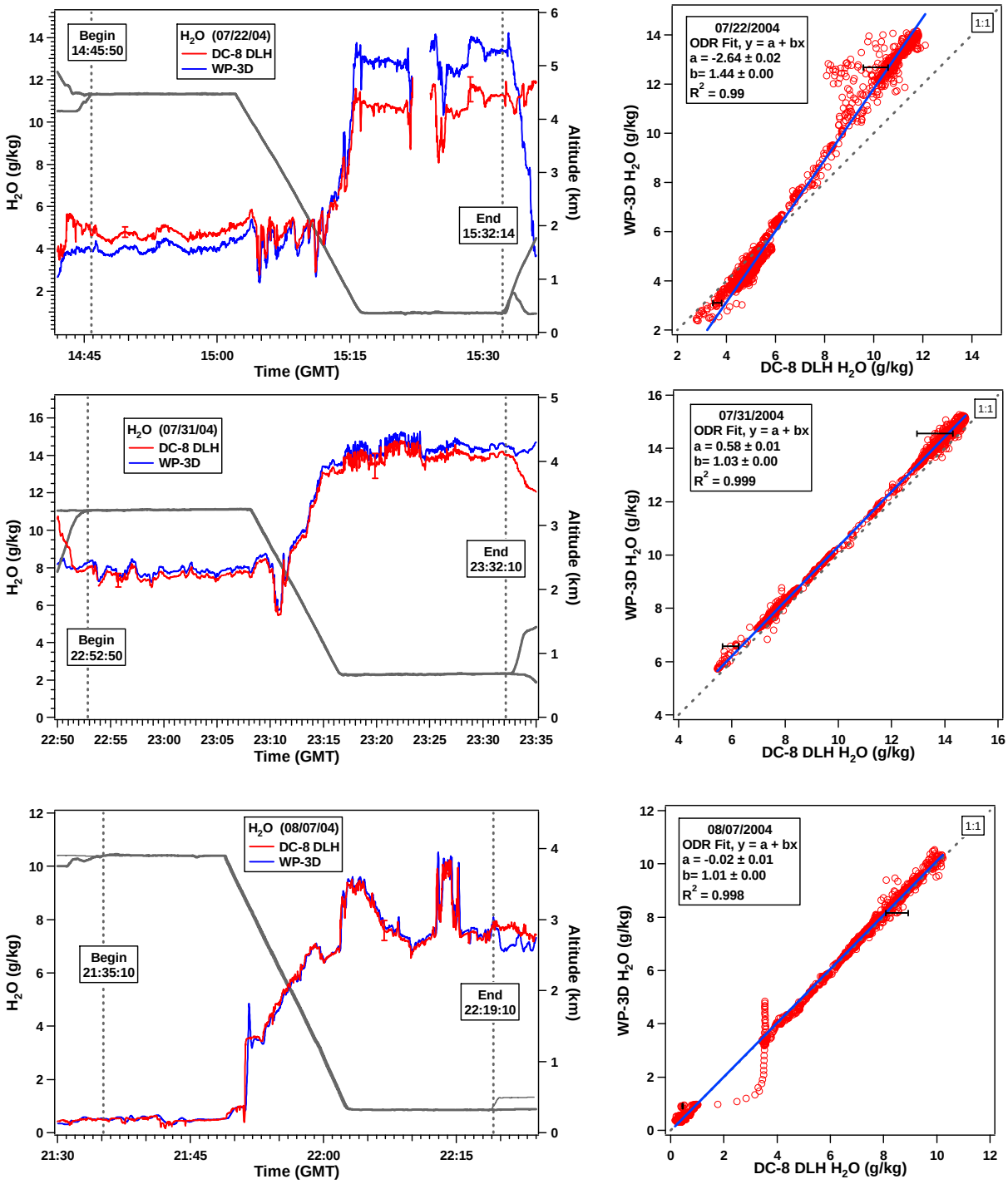

Figure 2. (left panels) Time series of DC-8 DLH and WP-3D cryo H_2O measurements and aircraft altitudes on the three intercomparison flights. (right panels) Correlations between the H_2O measurements on the two aircraft. Error bars shown depict the reported measurement uncertainties.

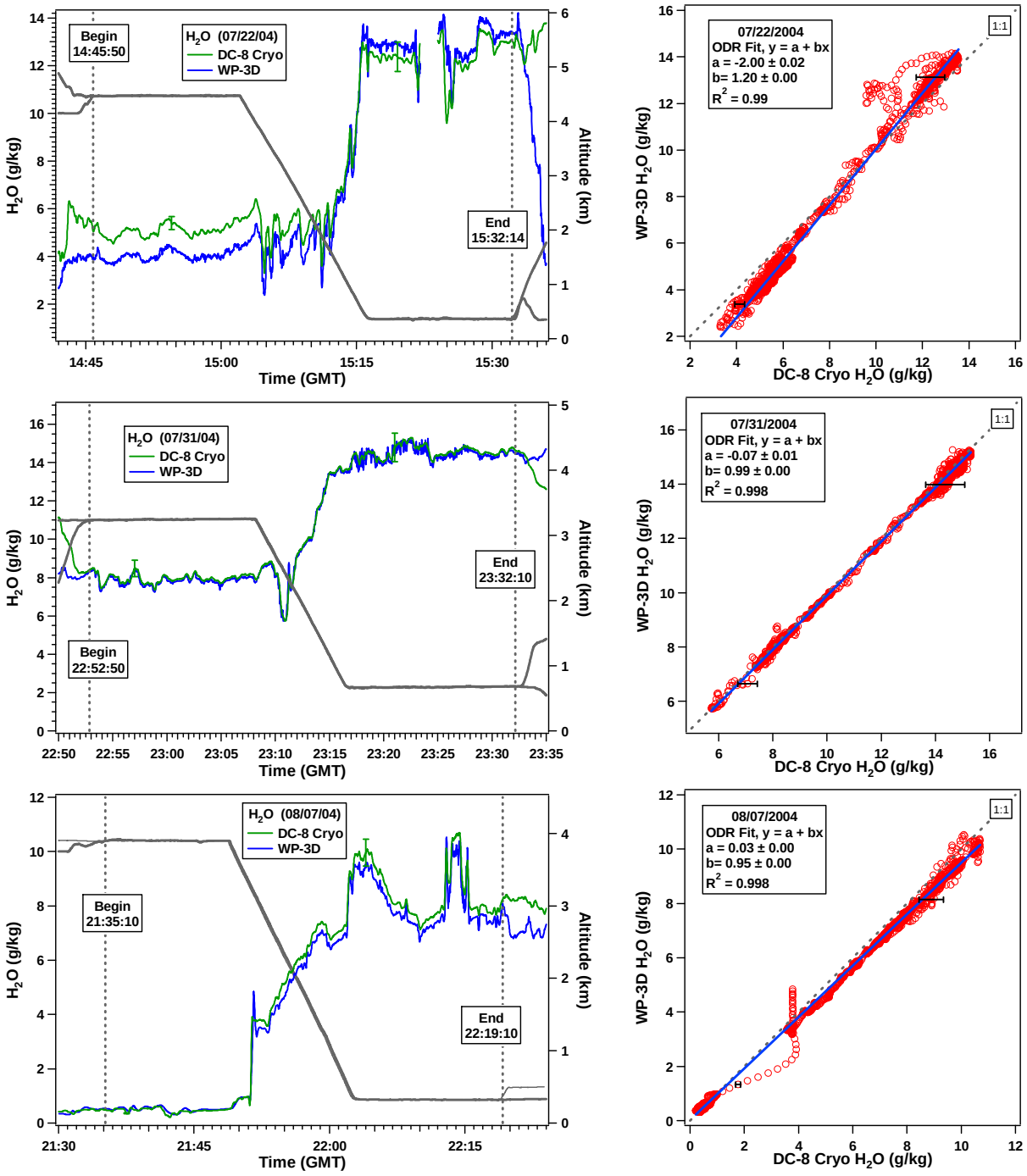

Figure 3. (left panels) Time series of DC-8 cryo and WP-3D cryo H_2O measurements and aircraft altitudes on the three intercomparison flights. (right panels) Correlations between the H_2O measurements on the two aircraft. Error bars shown depict the reported measurement uncertainties.

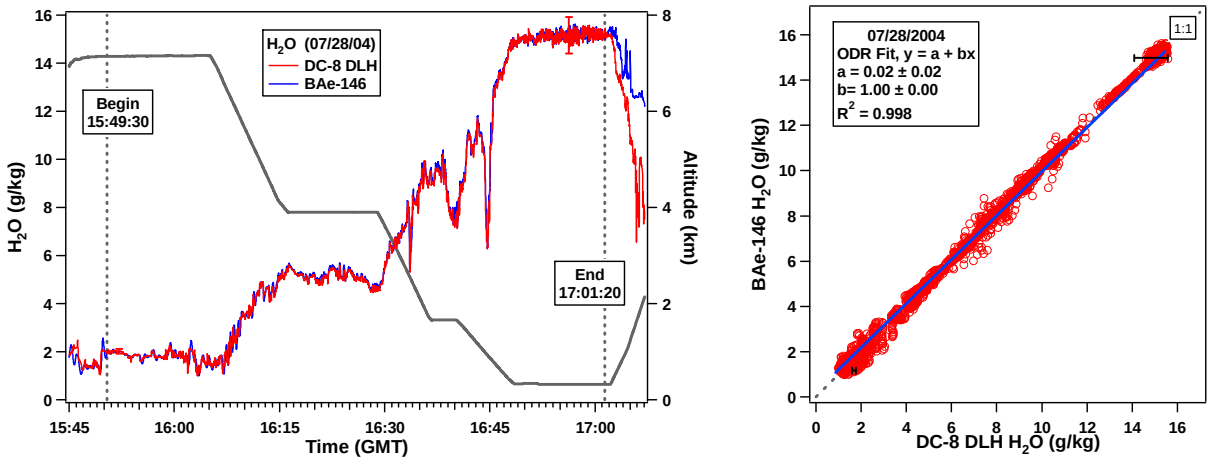

Figure 4. (left panel) Time series of H_2O measurements and aircraft altitudes from the intercomparison flight between the NASA DC-8 DLH and the FAAM BAe-146 hygro. (right panel) Correlations between the H_2O measurements on the two aircraft. Error bars shown depict the reported measurement uncertainties.

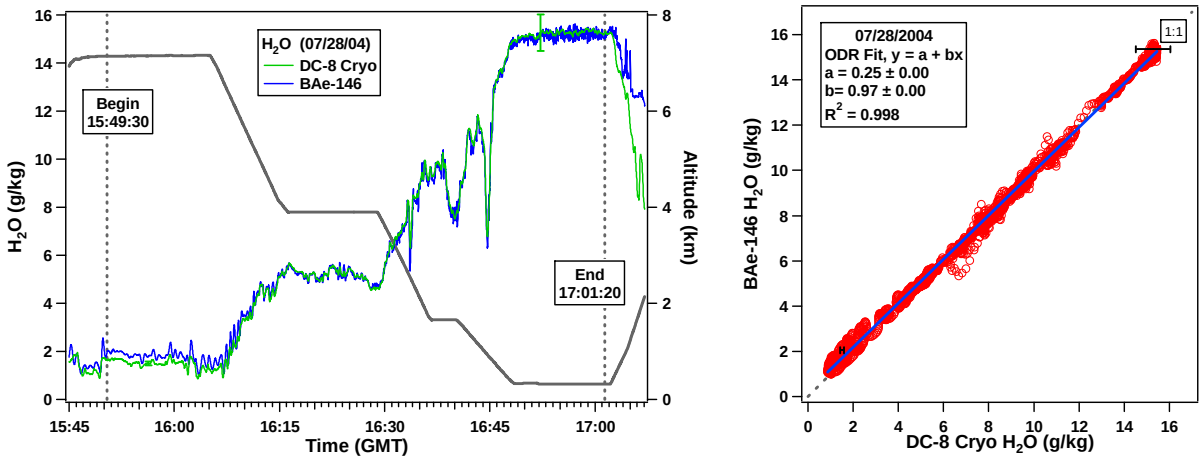

Figure 5. (left panel) Time series of H_2O measurements and aircraft altitudes from the intercomparison flight between the NASA DC-8 cryo and the FAAM BAe-146 hygro. (right panel) Correlations between the H_2O measurements on the two aircraft. Error bars shown depict the reported measurement uncertainties.

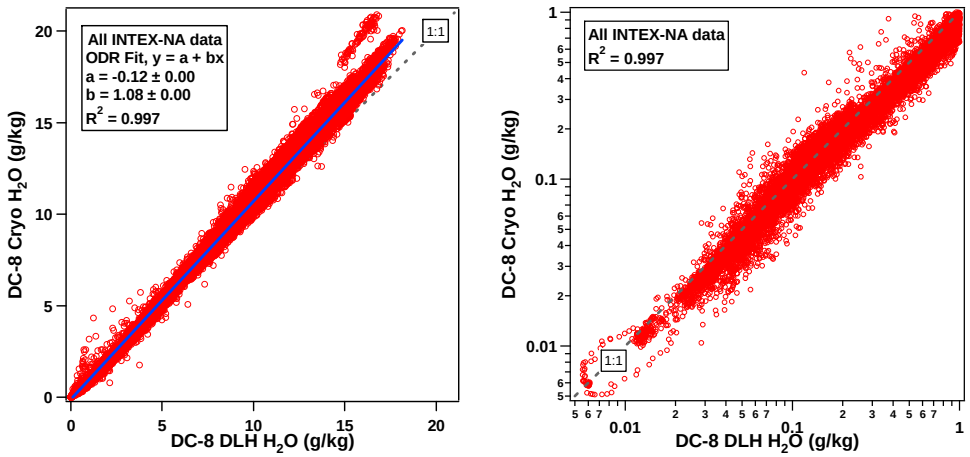

Figure 6. Correlation of DC-8 DLH and Cryo H_2O measurements for all INTEX-NA flights.

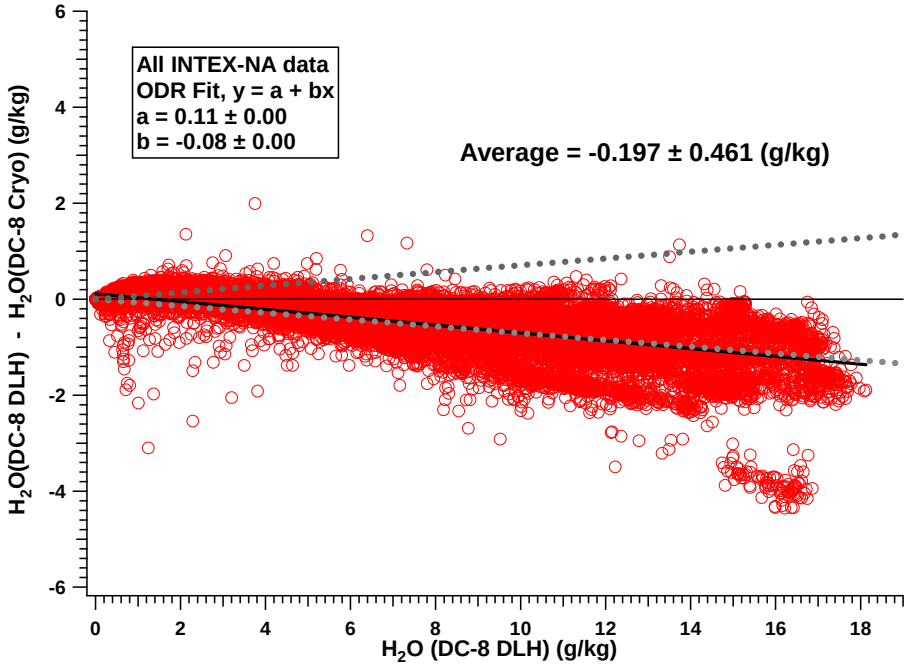

Figure 7. Difference between H_2O measurements from DC-8 DLH and DC-8 cryo for all intercomparison flights as a function of DC-8 DLH H_2O. The dashed lines indicate the range of the results expected from the reported 2σ measurement uncertainties.

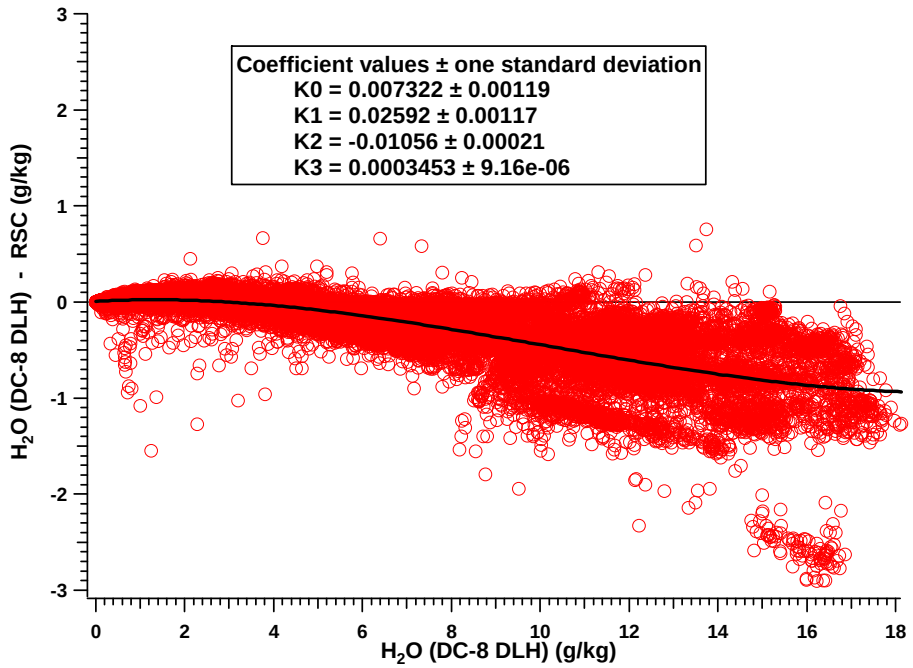

Figure 8. Difference between H_2O measurements from DC-8 DLH and RSC for all INTEX-NA flights as a function of DLH.

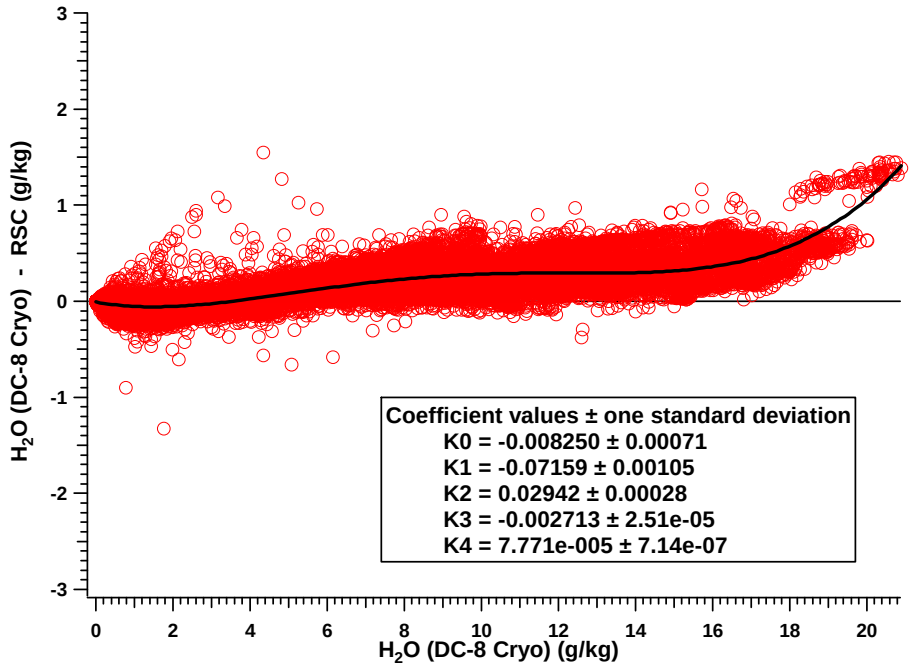

Figure 9. Difference between H_2O measurements from DC-8 cryo and RSC for all INTEX-NA flights as a function of DC-8 cryo.

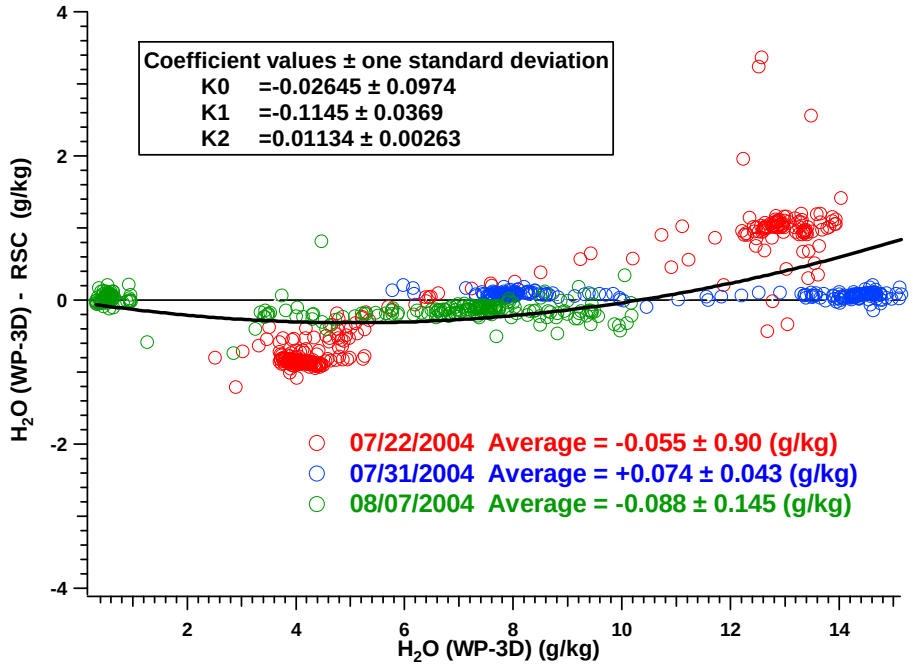

Figure 10. Difference between H_2O measurements from three DC-8/WP-3D intercomparison flights as a function of WP-3D H_2O. No uncertainty bounds are included because WP-3D did not report uncertainty.

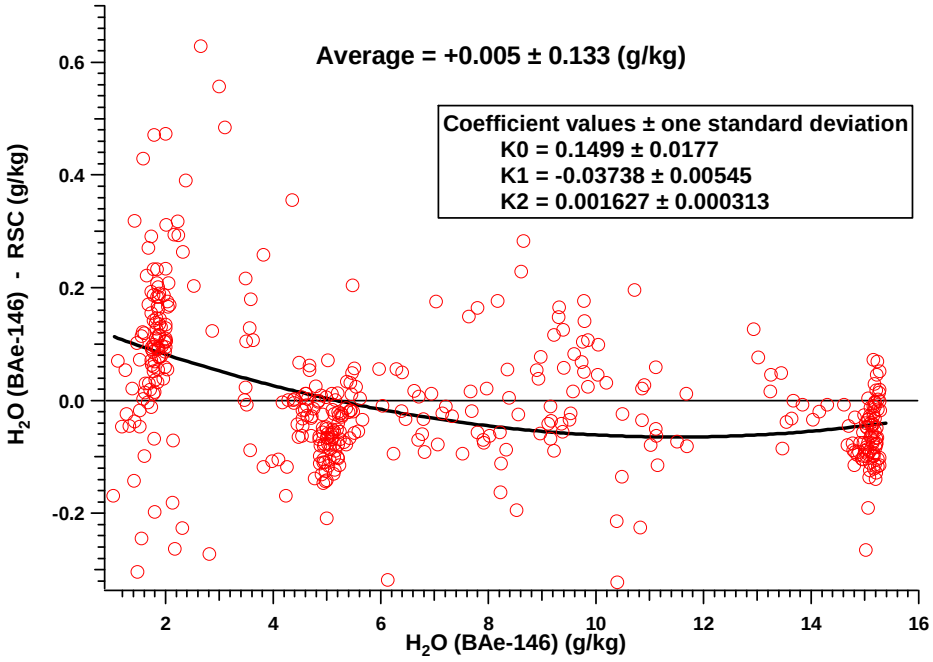

Figure 11. Difference between H_2O measurements from the DC-8/BAe-146 intercomparison flight (07/28) as a function of the BAe-146 H_2O. No uncertainty bounds are included because BAe-146 did not report uncertainty.

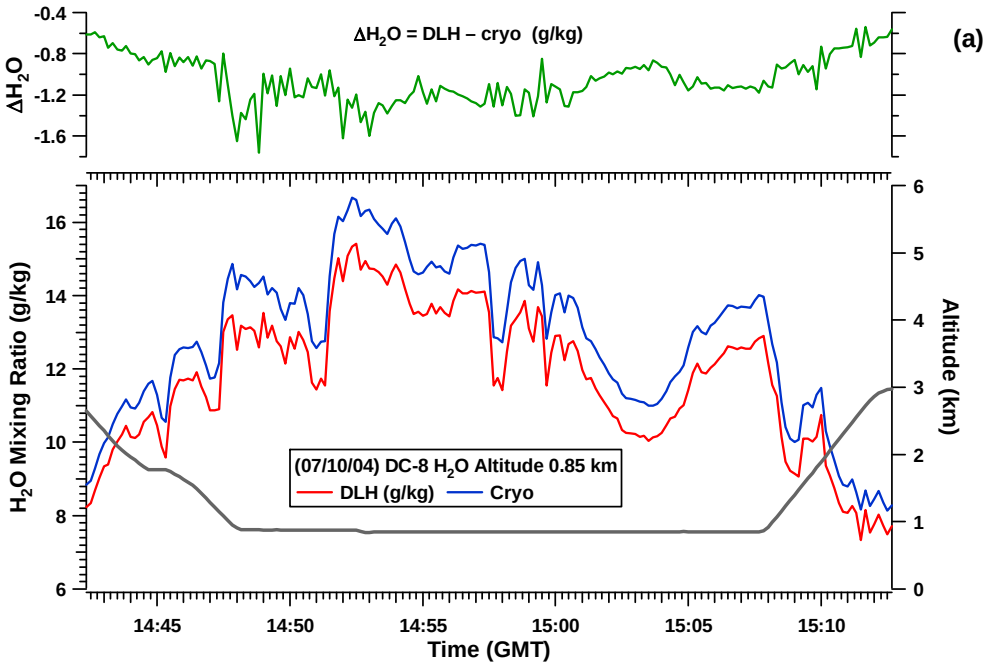
(a)
ΔH2O = DLH – cryo (g/kg)
ΔH2O
-0.4
-0.8
-1.2
-1.6
H2O Mixing Ratio (g/kg)
16
14
12
10
8
6
Altitude (km)
6
5
4
3
2
1
0
(07/10/04) DC-8 H2O Altitude 0.85 km
DLH (g/kg)
Cryo
14:45
14:50
14:55
15:00
15:05
15:10
Time (GMT)

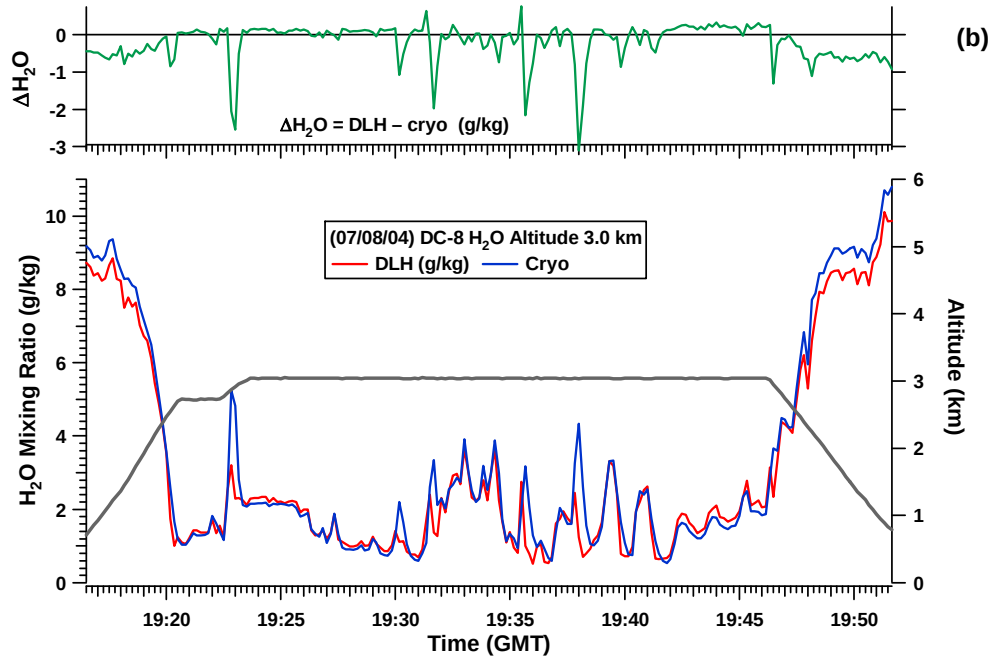
(b)
ΔH2O
0
-1
-2
-3
ΔH2O = DLH – cryo (g/kg)
H2O Mixing Ratio (g/kg)
10
8
6
4
2
0
Altitude (km)
6
5
4
3
2
1
0
(07/08/04) DC-8 H2O Altitude 3.0 km
DLH (g/kg)
Cryo
19:20
19:25
19:30
19:35
19:40
19:45
19:50
Time (GMT)

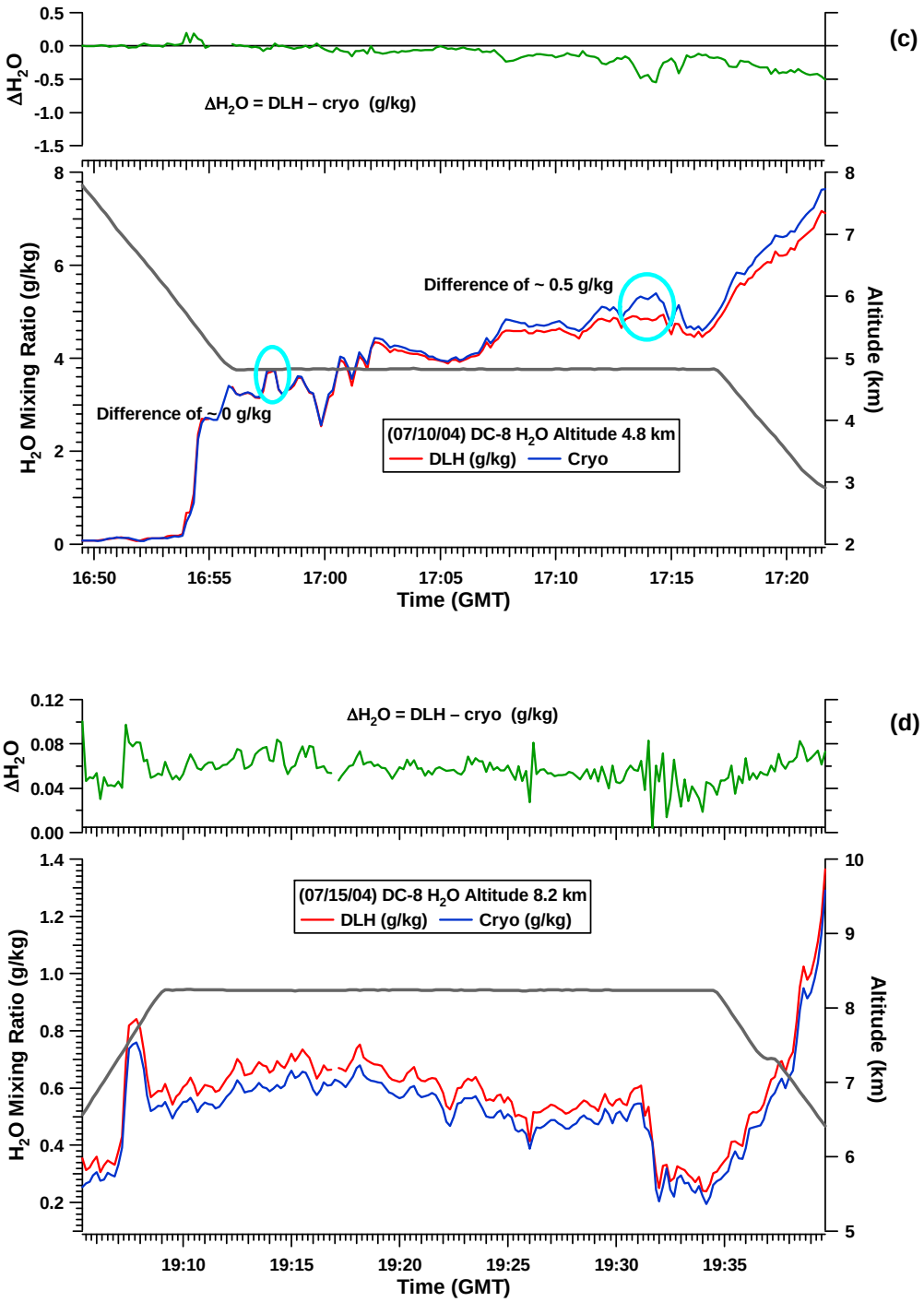

Figure 12. DC-8 DLH, cryo, and dew point during four level leg segments during flights on July 08 (b), July 10 (a and c), and July 15, 2004 (d).

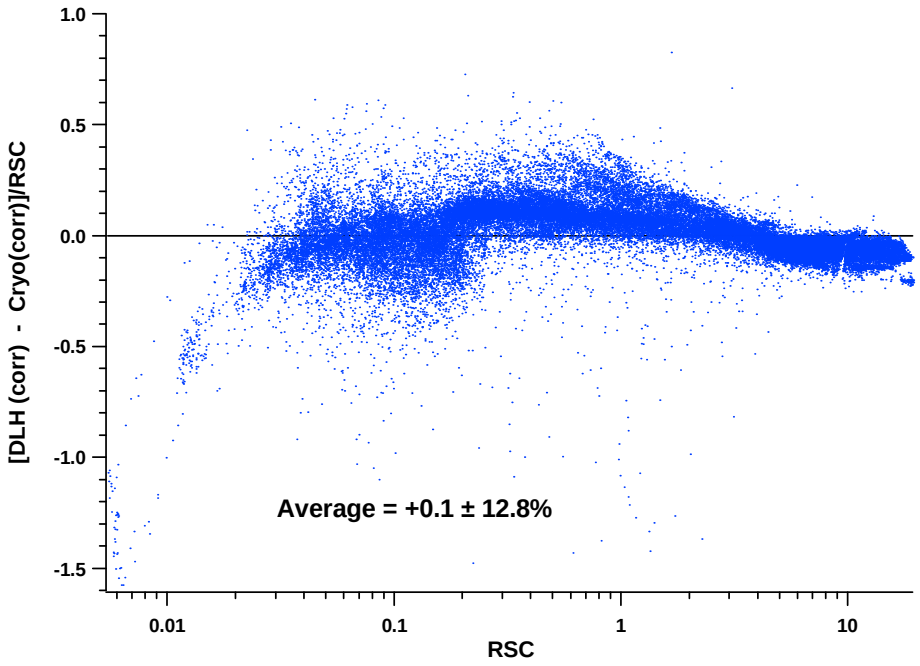

Figure 13. Relative difference between bias corrected H_2O measurements from DC-8 DLH and DC-8 Cryo for all INTEX-NA flights as a function of RSC.

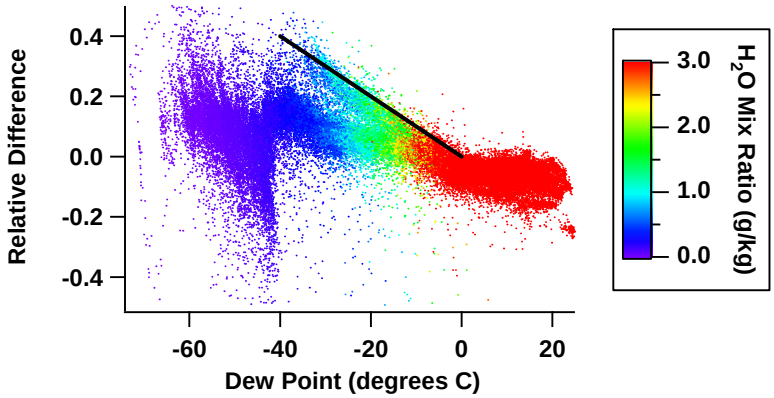

Figure 14. Relative difference between DC-8 DLH and cryo as a function of dew point.

References

Buck, A. L. and R. Clark, "Development of a Cryogenic Dew/Frost Point Hygrometer," Proc. American Meteorological Society, Jan 1991.

Diskin, G. S., et al. (2002), Open-Path Airborne Tunable Diode Laser Hygrometer, *Diode Lasers and Applications in Atmospheric Sensing*, SPIE Proceedings 4817, A. Fried, editor, 196-204.

Fehsenfeld, F. C., et al. (2006), International Consortium for Atmospheric Research on Transport and Transformation (ICARTT): North America to Europe—Overview of the 2004 summer field study, *J. Geophys. Res., 111*, D23S01, doi:10.1029/2006JD007829.

Singh, H. B., et al. (2006), Overview of the summer 2004 Intercontinental Chemical Transport Experiment-North America (INTEX-A), *J. Geophys. Res., 111*, D24S01, doi:10.1029/2006JD007905.